Sliding Mode Control of Induction Generator Wind Turbine Connected to the Grid

M. Ouassaid, K. Elyaalaoui and M. Cherkaoui

Abstract Conventional fossil fuels such as coal, oil and natural gas are being reduced and become more and more a source of serious undesirable effects on the environment. Wind power is playing a major role in the effort to augment the share of renewable energy sources in the world energy mix with a continuously increasing penetration into the grid. Wind turbine generators can be divided into two basic categories: fixed speed and variable speed. Variable-speed wind energy systems are presently favored than fixed-speed wind turbines thanks to their higher wind power extraction, improved efficiency, reactive power support and voltage control. This study addresses the problem of control of Wind Energy Conversion System (WECS) in variable speed. To this end, two simultaneous control objectives, namely the maximization of the energy conversion efficiency based on Squirrel Cage Induction Generator (SCIG) wind turbine and the regulation of the active and reactive power feed to the grid, to guarantee Unit Power Factor (UPF), have been established. To deal with the complexity and nonlinearity of the system, the sliding mode control is adopted. Indeed, this technique provides an efficient tool for controller design and presents attractive features such as robustness to parametric uncertainties of the different components of the system. In this way, sliding-mode control laws are developed using Lyapunov stability analysis, to guarantee the reaching and sustaining of sliding mode and stability of the system control. Evaluation of the reliability and performance of the proposed sliding mode control approach has been established on a 3MW three-blade wind turbine. Simulation results demonstrate that the proposed control strategy is effective in terms of MPPT control strategy, active and reactive power tracking trajectories and robustness against system parameter variations.

M. Ouassaid (✉) · K. Elyaalaoui · M. Cherkaoui
Ecole Mohammadia d'Ingénieurs, Mohammed V University, Rabat, Morocco
e-mail: ouassaid@emi.ac.ma

K. Elyaalaoui
e-mail: k.elyaalaoui@gmail.com

M. Cherkaoui
e-mail: cherkaoui@emi.ac.ma

1 Introduction

Currently, the demand for electric energy is growing rapidly. On the other hand, the conventional energy sources are depleting fast, their costs are going up, and they are causing the environment contamination. To meet these challenges, the attention has focused to renewable and clean energy sources, like wind, solar, fuel cell, etc. [6, 39].

Wind energy is an important renewable green energy resource. Indeed, it is omnipresent, environmentally friendly, and freely available [8]. Further, it is characterized by its high reliability and cost effectiveness. Thanks to all these features, the wind power generation capacity has been growing rapidly, with an average annual growth around 30 %, in the world, over the last decade.

Electric energy is generated from wind using a wind turbine and an electric generator. It can be used either for standalone loads or fed into the electric network through a suitable power electronic converters.

A wind turbine operates either at a fixed or variable speed.

- A fixed-speed wind turbine generator generally uses a squirrel-cage induction generator to convert the mechanical energy from the wind turbine into electrical energy (Fig. 1). The generator is connected directly to the electric network. The system operates almost at constant speed even if the wind speed varies. This topology is simple, less expensive and effective. But, it suffers from the low energy capture, mechanical stress and mediocre power quality [8, 20, 21, 25].
- Variable-speed wind turbine generator provides high efficiency in capturing the energy from wind over a wider range of wind speeds, along with better power quality. Also this scheme is capable to regulate the power factor, by either consuming
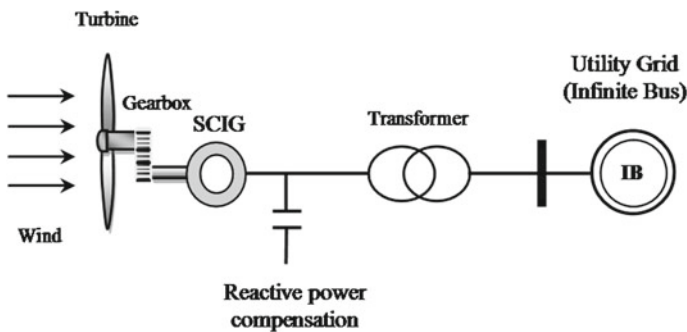

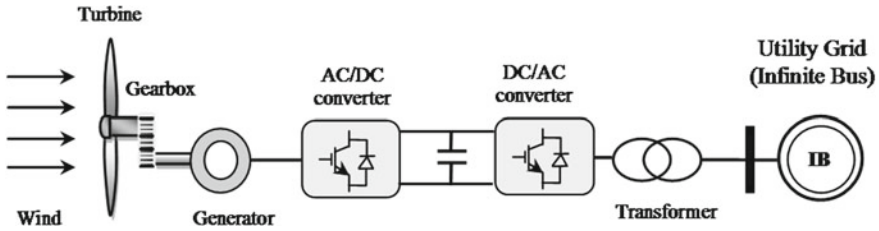**Fig. 1** Cage induction generator-based fixed speed wind turbine

Fig. 2 Variable speed wind turbine connected to a grid

or producing reactive power, and ensure lower mechanical stress. The power electronic converters are incorporated between the electrical machine and the power system as shown in Fig. 2 [22, 24, 33].

Most of the major wind turbine manufacturers are developing new megawatt scale wind turbines based on variable-speed operation with pitch control.

1.1 Wind Turbine Generators Technologies

Different types of electric machines are used for the generation of electric energy from wind:

- **Permanent Magnets Synchronous Generator (PMSG)**: The PM generators can be divided into radial-flux and axial-flux generators. The advantages of a PMSG configuration are gearless construction, the elimination of a dc excitation system, full controllability of the system for maximum wind power extraction and grid interface; and straightforward in accomplishing fault-ride through and grid support [7, 20, 21]. However, the major drawback of the PMSG is the high cost of the PM material and power converter [28].
- **Doubly-Fed Induction Generator (DFIG)—**wounded rotor: With this topology, the stator is connected directly to the grid whereas the rotor is linked to the grid via a bidirectional converter [27, 32]. The main characteristics of the DFIG are (i) limited operating speed range (ii) small scale power electronic converter (iii) reduced power losses and cost (vi) complete control of active and reactive power exchanged with the grid. However the most important disadvantages are necessity of gear and use of slip-rings which involve maintenance.
- **Squirrel Cage Induction Generator (SCIG)**: Induction generators were used for a long time for constant speed wind turbines. In this operating mode, the pitch control or active stall control are imposed for power limitation and protection. Currently, it is used for variable-speed wind energy systems which guarantee superior wind power extraction and better efficiency. In comparison with the DFIG, this configuration offers extended speed operating range, and complete decoupling between the generator and the network (Fig. 2), which results in higher power

extraction at different wind speeds and improved capability to realize the low-voltage ride-through. Indeed, SCIG provides some advantages when compared with the PMSG and DFIG such as light weight, small size, high reliability, maintenance less, high efficiency, low cost and operational simplicity [19, 36].

1.2 Control Technique Strategies of WECS

Wind generator and its control is a very complex electromechanical system. Linear controllers have been widely used in the engineering field for their reliability and simplicity. However, their parameters are usually tuned with the approximately linearized model. Consequently, the dynamic control performance may not be guaranteed during the transients of the wind turbine with WECS. To overcome these disadvantages, many methods for the design of controllers for the WECS have been investigated in order to ensure better control performance in terms of transient stability and robustness to parameter uncertainties or disturbances. These methods are summarized as follow:

- **Field Oriented Control (FOC)**. Common control of grid-connected WECS is based on FOC [1, 5]. The scheme decouples the stator current into active and reactive components in the synchronous reference frame. In this technique, the control of the system is accomplished by regulating the decoupled stator currents, using proportional-integral controllers [3]. However, the major disadvantage for this linear control scheme is that the performance may demean in the case of deviation of the machine parameters, such as stator and rotor inductances and resistances, from values used in the control system.
- **Feedback linearization**. The control based on this technique has been the subject of several investigations [14]. The aim of this method is to make the model of the system to be controlled exactly linearized by coordinate transformation using differential geometry theory. The obtained linearized system allows the synthesis of the control laws based on the linear optimal control principles. However, these control designs require precise models and often cancel some useful nonlinearities. Therefore, it does not guarantee the robustness in the presence of parameter uncertainties or disturbances. To overcome this drawback, numerous adaptive versions of the feedback linearizing techniques are then proposed [15, 38]. References [26, 41] present an application of this approach.
- **Backstepping technique**. This method offers an efficient tool for controller synthesis through building step by step the Lyapunov functions which can guarantee the asymptotic stability of the overall closed-loop system [17]. Indeed, the backstepping is less restrictive compared to the feedback linearization control which cancels the nonlinearities that might be useful. Unlike the adaptive controllers, based on certain equivalence, which separate the design of the controller and the terms of adaptation, adaptive backstepping has emerged as an alternative. This technique has been successfully applied for control of power system and wind power generator system in [3, 29, 30].

- **Direct Torque Control (DTC)**. In contrast to vector control with linear controllers (PI), DTC technique presents advantages such as simple structure and insensitivity to the parameters disturbances. The DTC technique directly controls machine torque and flux by selecting voltage vectors from a look-up-table using the stator flux and torque information. The problems with the DTC method is that (i) performances are very mediocre during starting and low-speed operation; (ii) converter switching frequency variation complicates the power circuit design; (iii) ripples in flux and torque [34]. This is due to the use of predefined switching table and hysteresis regulator. To deal with those drawbacks modified DTC strategies, incorporating space vector modulation, have been used to obtain constant switching frequency [16]. Nevertheless, further drawbacks were introduced, such as additional PI controller parameters, and sensitivity to system parameter variations [13, 18].
- **Direct Power Control (DPC)**. More recently, direct power control was developed based on the principles of DTC strategy. In [42], it was demonstrated that the control system is less complicated and robust against parameters machine variation. Nevertheless, switching frequency varies significantly with active and reactive power variations, rotor slip, and hysteresis bandwidth of power controllers. References [12, 34, 42] present an application of this technique.
- **Sliding-Mode Control (SMC)**. It is the most robust control techniques for systems with uncertainties and parameter variations. It dates back to the 70 s with the work of Utkin [40]. SMC features simple implementation, disturbance rejection, strong robustness, and fast responses. Nevertheless, the problems of chattering inherent in this type of discontinuous control appear quickly and may excite the highfrequency dynamics neglected sometimes leading to instability. Methods to tackle this phenomenon have been developed [35]. More recently, This technique has been successfully applied for wind power system in [10, 11, 23, 37].

In this study, a SMC strategy, for a variable speed wind turbine equipped with SCIG connected to the grid through power converters is developed:

- The prime control objective of the WECS is to capture the maximum wind power through MPPT control strategy. To this end, the turbine tip-speed ratio should be kept at its optimum value despite wind variations.
- The second objective consists of maintaining the DC bus voltage constant and to achieve the grid-side Unity Power Factor (UPF).

In the sections that follow, the chapter first introduces the mathematical model of different components of wind energy conversion system in Sect. 2. Then, Sect. 3 presents the synthesis of the control laws of the SCIG in order to maximize the wind energy conversion efficiency. Control design, of active and reactive power injected into the grid, is developed in Sect. 4. Section 5 presents the simulation results to demonstrate the performance of the proposed SMC strategy. Finally, the conclusions are made in Sect. 6.

2 Mathematical Model of Wind Energy Conversion System

The complete wind energy conversion system consists mainly of three parts: a wind turbine drive train, a SCIG, and two back-to back Voltage Source Converters (VSC). The system considered is shown in Fig. 3.

2.1 Model of Wind Turbine

The wind turbine basic principle is to convert the linear action of the wind into rotational energy. The converted energy is used to drive an electrical generator. Hence, the kinetic energy of the wind is transformed to electric power.

The wind power acting on the swept area of the blade A is a function of the air density ($1.225 \, \text{kg/m}^2$) and the wind speed V_w (m/s). The transmitted power Pw (w) is generally deduced from the wind power using the power coefficient C_p as [9]

$$P_w = \frac{1}{2}.C_p(\lambda, \beta) \cdot \rho \cdot A \cdot V_w^3 \tag{1}$$

The power coefficient is a nonlinear function of the tip speed-ratio λ, which depends on the wind velocity and the rotation speed of the shaft ω_t.
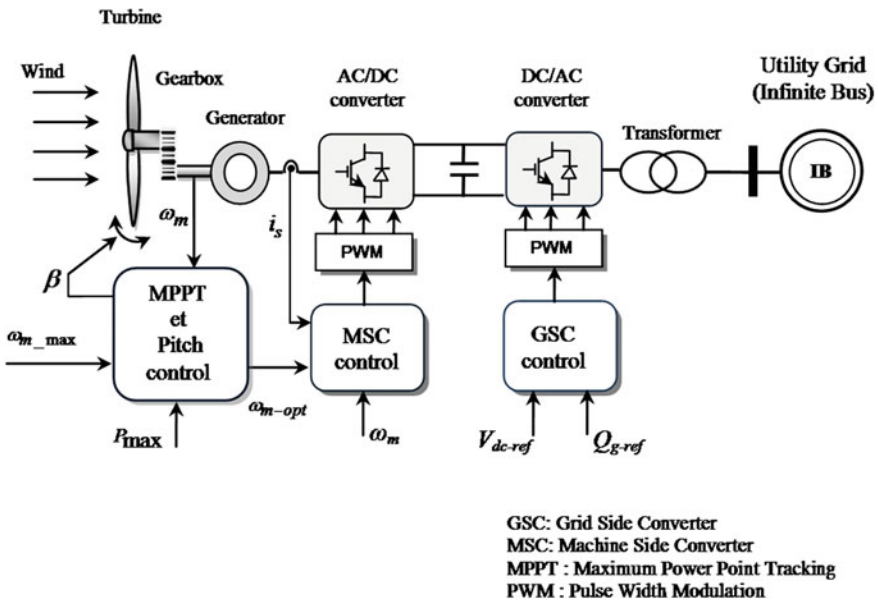

GSC: Grid Side Converter
MSC: Machine Side Converter
MPPT : Maximum Power Point Tracking
PWM : Pulse Width Modulation

Fig. 3 Control scheme of wind turbine based-SCIG connected to a grid

Table 1 Parameters of the coefficient of power

Symbole	C1	C2	C3	C4	C5	C6
Value	0.5109	116	0.4	5	21	0.0068

$$\lambda = \frac{R \cdot \omega_m}{V_w} \tag{2}$$

where R is the blade radius (m). The coefficient of power is expressed as

$$C_p(\lambda, \beta) = C_1 \left(\frac{C_2}{\lambda_i} - C_3 \cdot \beta - C_4 \right) \cdot \exp\left(\frac{-C_5}{\lambda_i} - C_6 \cdot \lambda \right)$$

$$\frac{1}{\lambda_i} = \frac{1}{\lambda + 0.08 \cdot \beta} - \frac{0.035}{\beta^3 + 1} \tag{3}$$

The parameters of coefficient of power are defined in Table 1.

Then, the input torque in the transmission mechanical system is given as

$$T_w = \frac{P_w}{\omega_t} = \frac{C_p(\lambda, \beta) \cdot \rho \cdot A \cdot V_w^3}{2\omega_t} \tag{4}$$

The maximum value of $C_p (\lambda, \beta)$ is $C_{pmax} = 0.47$ and obtained for $\lambda_{opt} = 8.1$ and for $\beta = 0°$. If the parameters are in pet unit, λ_{pu} and C_{p_pu} can be computed as

$$\lambda_{pu} = \frac{\lambda}{\lambda_{opt}}$$

$$C_{p\_pu} = \frac{C_p}{C_{p-opt}} \tag{5}$$

Both mechanical shafts are linked by the gearbox. The equation is expressed as [2]

$$2H\frac{d\omega_m}{dt} = T_m - T_e - F\omega_m \tag{6}$$

where $H = H_b + H_h + H_g$ is the inertia constant of the single rotating mass (which includes the blades, hub and generator rotor), ω_m is the rotor speed and F is the damping coefficient of a single mass.

2.2   Model of the Induction Generator

The generator, converting mechanical energy into electrical energy, is a SCIG with its stator windings connected to the grid through a frequency converter. The induction generator is described by 5th nonlinear mathematical model, in the space vector by the following state-space form [3, 20, 21]

$$\frac{1}{\omega_b}\frac{di_{sd}}{dt} = -\partial_1 i_{sd} + \omega_s i_{sq} - \partial_2 \phi_{rd} - \frac{V_{sd}}{\sigma L_s} \tag{7}$$

$$\frac{1}{\omega_b}\frac{di_{sq}}{dt} = -\partial_1 i_{sq} - \omega_s i_{sd} + \partial_3 \phi_{rd} - \frac{V_{sq}}{\sigma L_s} \tag{8}$$

$$\frac{1}{\omega_b}\frac{d\phi_{rd}}{dt} = -\frac{R_r \phi_{rd}}{L_r} - \frac{R_r L_m}{L_r} i_{sd} \tag{9}$$

$$\frac{1}{\omega_b}\frac{d\phi_{rq}}{dt} = -\frac{R_r L_m}{L_r} i_{sq} - (\omega_s - \omega_m)\phi_{rd} \tag{10}$$

$$2H\frac{d\omega_m}{dt} = -\frac{L_m}{L_r}\phi_{rd} i_{sq} + T_m - F\omega_m \tag{11}$$

where

$$\partial_1 = \frac{R_s L_r^2 + R_r L_m^2}{\sigma L_s L_r^2}, \partial_2 = \frac{R_r L_m}{\sigma L_s L_r^2}, \partial_3 = \frac{L_m \omega_m}{\sigma L_s L_r}, \quad L_r = L_{\sigma r} + L_m \quad \text{and} \quad L_s = L_{\sigma s} + L_m$$

$L_{\sigma r}$ and $L_{\sigma r}$ are the leakage inductances of stator and rotor, L_m is the mutual inductance. $\omega_b = 2\pi f$ is the system base frequency, ω_s is the synchronous electrical speed, ω_m is the rotor speed of the SCIG.

Remark The nonlinear control is applied to orient rotor flux on d-axis of the rotating reference frame, therefore, $\Phi_{rq} = 0$ and $\Phi_{rd} = \Phi_{ref}$.

2.3 Model of the Converters

The frequency converter is built by two current-regulated voltage-source pulse width modulation (PWM) converters: a Machine Side Converter (MSC) and a Grid Side Converter (GSC), with a dc voltage link in between.

The modeling of the converters is made by using the concept of instantaneous average value. The converter is equivalent to a matrix topology as given in (12).

$$\begin{bmatrix} V_{sa} \\ V_{sb} \\ V_{sc} \end{bmatrix} = \frac{V_{dc}}{3}\begin{bmatrix} 2 & -1 & -1 \\ -1 & 2 & -1 \\ -1 & -1 & 2 \end{bmatrix}\begin{bmatrix} S_a \\ S_b \\ S_c \end{bmatrix} \tag{12}$$

S_a, S_b, S_c are variables which represent the switching status and take the value 1 when the switch is closed (on) and 0 when it is opened (off).

The model of DC link voltage is given as [4]

$$Cv_{dc}\frac{dv_{dc}}{dt} = P_{ge} - P_{gr} \tag{13}$$

where C is the capacitance, P_{ge} is the active power of generator and P_{gr} is the active power injected into AC network.

2.4 The Model of the Filter

The SCIG is connected to the grid through a filter. The model of the filter is given by [20, 21]

$$v_{fd} = L_f\frac{di_{fd}}{dt} + R_f i_{fd} - L_f\omega_e i_{fq} + e_d \tag{14}$$

$$v_{fq} = L_f\frac{di_{fq}}{dt} + R_f i_{fq} + L_f\omega_e i_{fd} + e_q \tag{15}$$

where L_f and R_f are the filter inductance and filter resistance respectively; v_{fd} and v_{fq} are the filter voltage components of d-axis and q-axis respectively, e_d and e_q are the grid voltage components of d-axis and q-axis respectively, i_{fd} and i_{fq} are the values of the current of d axis and q-axis respectively, and $\omega_e = 2\pi f$ where f is the grid frequency.

3 Nonlinear Control of SCIG

A generator side converter connected to the stator of the SCIG effectively decouples the generator from the grid. Hence, the generator rotor speed depends only on the wind conditions.

The first control objective is to track the optimum generator speed ω_{m_opt} and to orient the rotor flux on the d-axis.

3.1 Control of Generator Speed

The optimum generator speed ω_{m_opt} is generated by a MPPT technique to determine the stabilizing function. The tracking error between speed and its reference is given as

$$e_1 = \omega_{m\_opt} - \omega_m \tag{16}$$

The sliding surface is chosen as follow

$$S_1(t) = K_1 e_1(t) \tag{17}$$

where K_1 is a positive constant feedback gain.

In order to satisfy the sliding mode existence law, the control input is chosen to have the following structure

$$u(t) = u_{eq}(t) + u_n(t) \tag{18}$$

where $u_{eq}(t)$ is an equivalent control-input that determines the system's behavior on the sliding surface and $u_n(t)$ is a non-linear switching input, which drives the state to the sliding surface and maintains the state on the sliding surface in the presence of the parameter variations and disturbances [31, 40]. The equivalent control-input is obtained from the invariance condition and is given by the following condition $S_1 = 0$ and $\frac{dS}{dt} = 0 \Rightarrow u(t) = u_{eq}(t)$.

Hence the derivative of the sliding surface (17) is given as

$$\begin{aligned}
\frac{dS_1(t)}{dt} &= K_1 \left(\frac{d\omega_{m\_opt}}{dt} - \frac{d\omega_m}{dt} \right) \\
&= K_1 \frac{d\omega_{m\_opt}}{dt} + \frac{K_1}{2H} \left(\frac{L_m \varphi_{ref}}{L_r} i_{sq} - T_m + F\omega_m \right)
\end{aligned} \tag{19}$$

The i_{sq} can be viewed as a virtual control in the above equation. It is derived to ensure the SCIG speed convergence to the optimum speed. To ensure the Lyapunov stability criteria i.e. $\frac{dS_1}{dt} S_1 \prec 0$, the nonlinear control input i_{sq_eq} is defined as

$$i_{sq\_eq} = \left(-2H \frac{d\omega_{m\_opt}}{dt} + T_m - F\omega_m \right) \frac{L_r}{L_m \varphi_{ref}} \tag{20}$$

The nonlinear switching input i_{sq-n} can be chosen as follows

$$i_{sq-n} = -\alpha_1 \frac{2HL_r}{L_m \varphi_{ref}} \operatorname{sgn}(e_1) \tag{21}$$

where α_1 is a positive constant and the sign function is defined to reduce the phenomenon of charting as

$$\operatorname{sgn}(S(t)) = \frac{S(t)}{|S(t)| + \varepsilon} \tag{22}$$

where ε is a small positive number. Then, the reference of q-axis current is expressed as

$$i_{sq\_ref} = \left(-2H \frac{d\omega_{m\_opt}}{dt} + T_m - F\omega_m - 2H\alpha_1 \operatorname{sgn}(e_1) \right) \frac{L_r}{L_m \phi_{ref}} \tag{23}$$

Substituting (23) in (19), the q-axis current sliding surface dynamics becomes

$$\frac{dS_1(t)}{dt} = -K_1\alpha_1 \operatorname{sgn}(e_1) \tag{24}$$

3.2 Control of d-Axes Rotor Flux

The d-axis rotor flux Φ_{rd} can be estimated from Eq. (9) as

$$\phi_{rd-estim} = -\frac{L_m}{1 + T_r \cdot s} i_{sd} \tag{25}$$

where $T_r = \frac{\omega_b L_r}{R_r}$ is the time constant.

  The stabilizing error between ϕ_{rd} and its desired trajectory ϕ_{ref} is defined as

$$e_2(t) = \phi_{ref} - \phi_{rd} \tag{26}$$

To stabilize the d-axis rotor flux Φ_{rd}, the new sliding surface is selected as

$$S_2(t) = K_2 e_2(t) \tag{27}$$

where K_2 is a positive constant. The derivative of $S_2(t)$ using (9) and (27) is given as

$$\frac{dS_2(t)}{dt} = K_2\frac{d\phi_{ref}}{dt} + K_2\omega_b\frac{R_r}{L_r}[\phi_{rd} + L_m i_{sd}] \tag{28}$$

Then, the equivalent control i_{sd_eq} (29) is obtained as the solution of the equation $\frac{dS_2(t)}{dt} = 0$.

$$i_{sd\_eq} = -\frac{L_r}{\omega_b L_m R_r}\frac{d\phi_{ref}}{dt} - \frac{1}{L_m}\phi_{rd} \tag{29}$$

As a result, the stabilizing function of the control current is defined as

$$i_{sd\_ref} = -\frac{L_r}{\omega_b L_m R_r}\frac{d\phi_{ref}}{dt} - \frac{1}{L_m}\phi_{rd} - \frac{L_r}{\omega_b L_m R_r}\alpha_2 \operatorname{sgn}(e_2) \tag{30}$$

where α_2 is a positive constant. Using (30), the d-axis current sliding surface dynamics (28) becomes

$$\frac{dS_2(t)}{dt} = -K_2\alpha_2 \operatorname{sgn}(e_2) \tag{31}$$

Since the d-axis current and the q-axis current are not our control inputs, the stabilizing errors between i_{sd_ref} and i_{sq_ref} and their desired trajectories, respectively, are defined as

$$e_3(t) = i_{sd\_ref}(t) - i_{sd}(t) \tag{32}$$

$$e_4(t) = i_{sq\_ref}(t) - i_{sq}(t) \tag{33}$$

To stabilize $i_{sd}(t)$ and $i_{sq}(t)$, the new sliding surfaces are selected as

$$\begin{cases} S_3(t) = K_3 e_3(t) \\ S_4(t) = K_4 e_4(t) \end{cases} \tag{34}$$

where K_3 and K_4 are a positive constants. Then, the derivative of sliding surfaces are defined as

$$\frac{dS_3(t)}{dt} = K_3 \left(\frac{di_{sd\_ref}}{dt} - \frac{di_{sd}}{dt} \right) \tag{35}$$

$$\frac{dS_4(t)}{dt} = K_4 \left(\frac{di_{sq\_ref}}{dt} - \frac{di_{sq}}{dt} \right) \tag{36}$$

when replacing (7) in (35) and (8) in (36), then track the same steps used to obtain the control currents, the control voltage laws are obtained as

$$V_{sd\_ref} = \sigma L_s \left(-\frac{1}{\omega_b} \frac{di_{sd\_ref}}{dt} - \partial_1 i_{sd} + \omega_s i_{sq} - \partial_2 \phi_{rd} - \frac{\alpha_3}{\omega_b} \operatorname{sgn}(e_3(t)) \right) \tag{37}$$

$$V_{sq\_ref} = \sigma L_s \left(-\frac{1}{\omega_b} \frac{di_{sq\_ref}}{dt} - \partial_1 i_{sq} - \omega_s i_{sd} + \partial_3 \phi_{rd} - \frac{\alpha_4}{\omega_b} \operatorname{sgn}(e_4(t)) \right) \tag{38}$$

3.3   Stability Analysis

Theorem 1 *The dynamic sliding mode control laws (37) and (38) with stabilizing functions (23) and (30) when applied to the SCIG side converter, guarantee the asymptotic convergence of the generator speed ω_m and the d-axis rotor flux Φ_{rd} to their desired values ω_{m_opt} and ϕ_{ref}, respectively.*

Proof Consider the following positive definite Lyapunov function

$$V_1 = \frac{1}{2} S_1^2 + \frac{1}{2} S_2^2 + \frac{1}{2} S_3^2 + \frac{1}{2} S_4^2 \tag{39}$$

By considering (24), (31), (35) and (36), the derivative of (39) can be derived as follows

$$
\begin{aligned}
\frac{dV_1}{dt} &= \frac{dS_1}{dt}S_1 + \frac{dS_2}{dt}S_2 + \frac{dS_3}{dt}S_3 + \frac{dS_4}{dt}S_4 \\
&= -K_1^2\alpha_1 e_1 \operatorname{sgn}(e_1) - K_2^2\alpha_2 e_2 \operatorname{sgn}(e_2) \\
&\quad + K_3^2 e_3 \left(\frac{di_{sd\_ref}}{dt} - \frac{di_{sd}}{dt}\right) + K_4^2 e_4 \left(\frac{di_{sq\_ref}}{dt} - \frac{di_{sq}}{dt}\right)
\end{aligned}
\tag{40}
$$

Substituting the control laws (37) and (38) in (40) gives

$$
\begin{aligned}
\frac{dV_1}{dt} &= -K_1^2\alpha_1 e_1 \operatorname{sgn}(e_1(t)) - K_2^2\alpha_2 e_2 \operatorname{sgn}(e_2(t)) \\
&\quad - K_3^2\alpha_3 e_3 \operatorname{sgn}(e_3(t)) - K_4^2\alpha_4 e_4 \operatorname{sgn}(e_4(t)) \\
&= -\sum_{i=1}^{4} \alpha_i K_i^2 |e_i| < 0
\end{aligned}
\tag{41}
$$

From the above analysis, it is evident that the reaching condition of sliding mode is guaranteed.

4 Sliding Mode Control of Grid Side Converter

The aim of the grid side converter control is to maintain the dc link voltage constant, thereby ensuring that the active power generated by the SCIG is fed to the grid. Also this control must be able to provide perfect tracking performance of the reactive power fed to the network to its reference trajectory.

4.1 Control Laws of Reactive and Active Powers

By orienting the grid voltage space vector on the d axis, we obtain

$$
\begin{aligned}
e_d &= V \\
e_q &= 0
\end{aligned}
\tag{42}
$$

Substituting (42) in (14) and (15) gives the following equations of the filter

$$
\frac{di_{fd}}{dt} = \frac{1}{L_f}\left(v_{fd} - R_f i_{fd} + L_f \omega_e i_{fq} - V\right)
\tag{43}
$$

$$\frac{di_{fq}}{dt} = \frac{1}{L_f} \left(v_{fq} - R_f i_{fq} - L_f \omega_e i_{fd} \right) \tag{44}$$

The reactive power and active power of grid can be expressed as

$$P_{gr} = i_{fd} V \tag{45}$$

$$Q_{gr} = i_{fq} V \tag{46}$$

From (45) and (46), it can be seen that the active and reactive power of grid can be controlled by the direct and quadrature components current, respectively. Then, let's define

$$e_5(t) = i_{fd\_ref} - i_{fd} \tag{47}$$

$$e_6(t) = i_{fq\_ref} - i_{fq} \tag{48}$$

where i_{fd_ref} and i_{fq_ref} are the desired values of the i_{fd} and i_{fq}. The current i_{fd_ref} is derived directly from the control loop of the DC bus voltage, while i_{fq_ref} is computed by (48). Q_{gr} is set to zero in order to ensure unit power factor $i_{fq\_ref} = 0$. The sliding surface for i_{fd} and i_{fq} can be expressed as

$$S_5(t) = K_5 e_5(t) \tag{49}$$

$$S_6(t) = K_6 e_6(t) \tag{50}$$

The DC bus voltage is regulated by using the proportional integral (PI) regulator. The derivative of (49) and (50) using (43) and (44) gives

$$\frac{dS_5(t)}{dt} = K_5 \left(\frac{di_{fd\_ref}}{dt} - \frac{1}{L_f} \left(v_{fd} - R_f i_{fd} + L_f \omega_e i_{fq} - V \right) \right) \tag{51}$$

$$\frac{dS_6(t)}{dt} = K_6 \left(\frac{di_{fq\_ref}}{dt} - \frac{1}{L_f} \left(v_{fq} - R_f i_{fq} - L_f \omega_e i_{fd} \right) \right) \tag{52}$$

To ensure the reaching condition $\frac{dS_5}{dt} S_5 \prec 0$, the equivalent control $v_{fd-eq}(t)$ is obtained as

$$v_{fd-eq} = L_f \frac{di_{fd\_ref}}{dt} + R_f i_{fd} - L_f \omega . i_{fq} + V \tag{53}$$

Subsequently, the control law is written as follows

$$v_{fd} = L_f \frac{di_{fd\_ref}}{dt} + R_f i_{fd} - L_f \omega . i_{fq} + V + \alpha_5 \operatorname{sgn}(e_5(t)) \tag{54}$$

In the same way, the control voltage law for the reactive power tracking is given as

$$v_{fq} = L_f \frac{di_{fq\_ref}}{dt} + R_f i_{fq} + L_f \omega.i_{fd} + L_f \alpha_6 \, \mathrm{sgn}(e_6(t)) \tag{55}$$

4.2 Stability Analysis

Theorem 2 *The dynamic sliding mode control laws (54) and (55) when applied to the grid side converter, guarantee the asymptotic convergence of the reactive and active powers to their reference trajectories P_{gr} and $Q_{gr} = 0$, respectively.*

Proof Consider the following positive definite Lyapunov function

$$V_2 = \frac{1}{2}S_5^2 + \frac{1}{2}S_6^2 \tag{56}$$

By considering (51) and (52) the derivative of (56) can be derived as follows

$$
\begin{aligned}
\frac{dV_2}{dt} &= \frac{dS_5}{dt}S_5 + \frac{dS_6}{dt}S_6 \\
&= K_5^2 e_5 \left(\frac{di_{fd\_ref}}{dt} - \frac{1}{L_f}\left(v_{fd} - R_f i_{fd} + L_f \omega_e i_{fq} - V\right)\right) \\
&\quad + K_6^2 e_6 \left(\frac{di_{fq\_ref}}{dt} - \frac{1}{L_f}\left(v_{fq} - R_f i_{fq} - L_f \omega_e i_{fd}\right)\right)
\end{aligned} \tag{57}
$$

Substituting the control laws (54) and (55) in (57) gives

$$
\begin{aligned}
\frac{dV_2}{dt} &= -\alpha_5 K_5^2 e_5 \, \mathrm{sgn}\,(e_5(t)) - \alpha_6 K_6^2 e_6 \, \mathrm{sgn}(e_6(t)) \\
&= -\alpha_5 K_5^2 \, |e_5| - \alpha_6 K_6^2 \, |e_6| \\
&\leq 0
\end{aligned} \tag{58}
$$

Therefore the condition of sliding mode of the system is guaranteed.

5 Simulation Results and Discussion

A 3 MW, 690 V SCIG wind turbine system is simulated in the MATLAB/Simulink software environment to demonstrate the effectiveness of the proposed control scheme. The SCIG wind turbine is modeled by 5th nonlinear mathematical model.
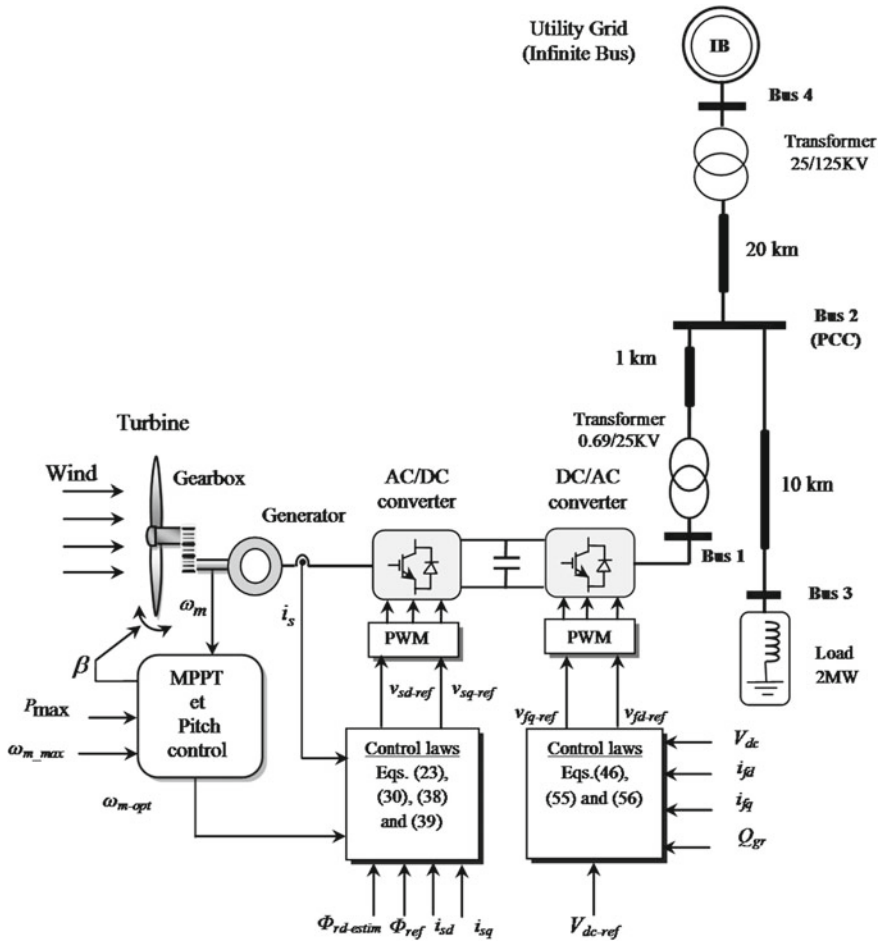
Fig. 4 Schematic diagram of the proposed control of SCIG wind turbine

The MSC and the GSC are represented by a switch-level model in which the operation of each individual switch is fully represented. Figure 4 shows the scheme of the implemented system. The parameters of the SCIG wind turbine are given in the Table 2.

The power reference is generated by a maximum power point tracking (MPPT) algorithm that searches for the peak power on the power–speed curve.

Table 2 Parameters of the wind turbine SCIG

Symbol	Quantity	Value
P_r	Rated power	3 (MW)
V_s	Rated voltage	690 (V)
F	Rated frequency	50 (Hz)
R_s	Stator resistance	0.004843 (pu)
L_s	Stator leakage Inductance	0.1248 (pu)
R_r	Rotor resistance	0.004347 (pu)
L_r	Rotor leakage Inductance	0.1791 (pu)
L_m	Mutual inductance	6.77 (pu)
H	Per unit Inertia constant	3.04 (pu)
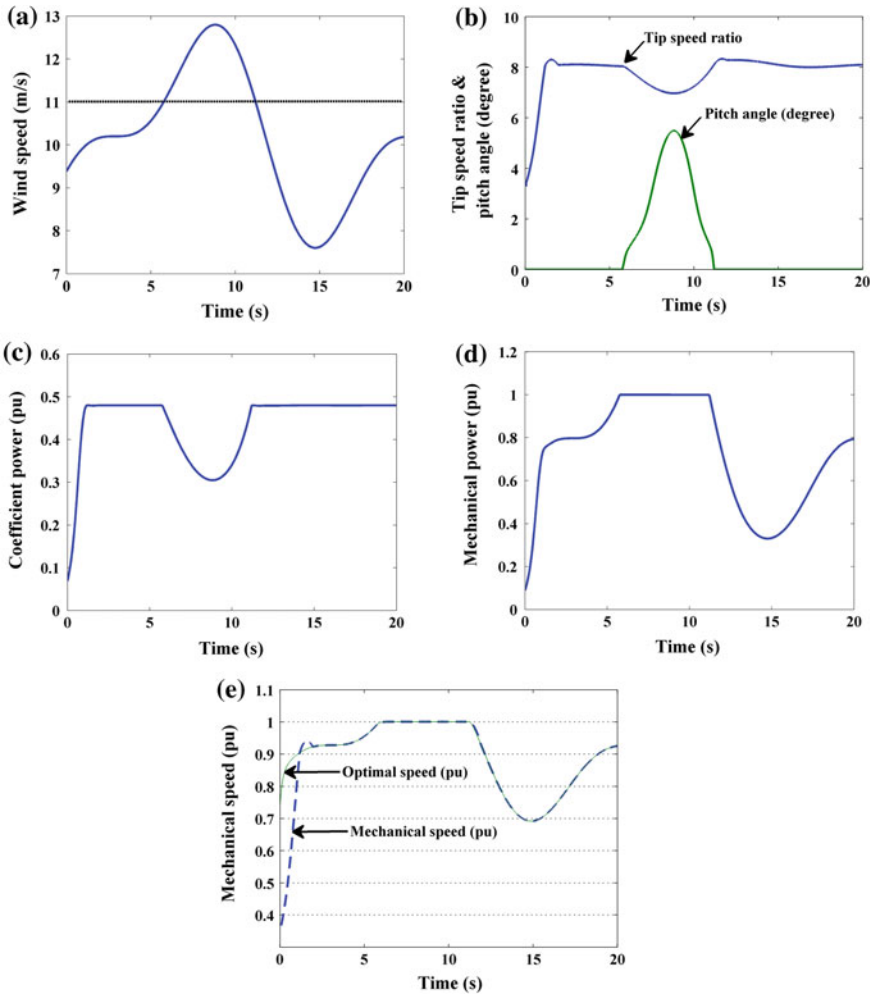
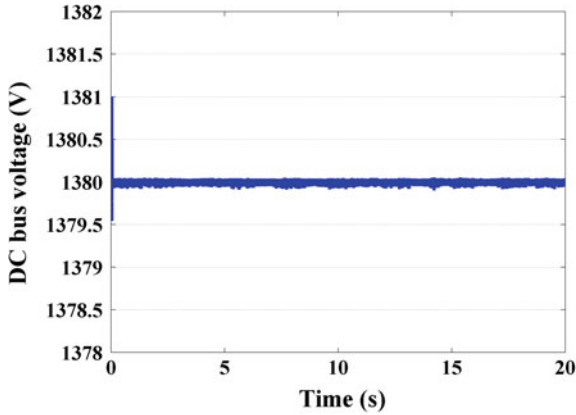**Fig. 5** Simulation results of MPPT control of SCIG wind turbine

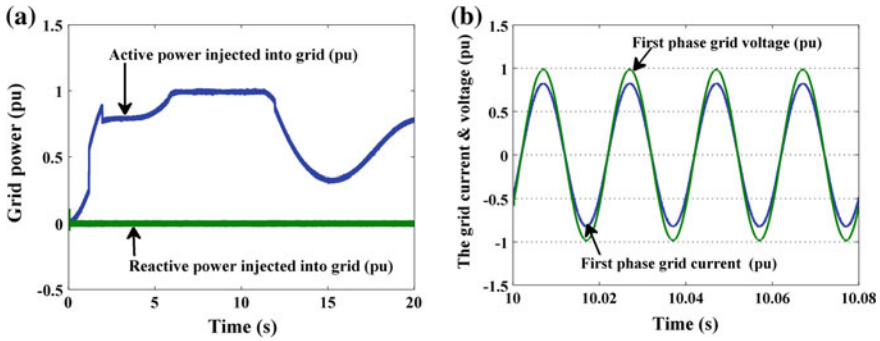**Fig. 6** Illustration of tracking performance of DC link voltage

Fig. 7 Performance tracking of power and wave forms of grid voltage and current

5.1 Responses of MPPT Control

To extract maximum power corresponding to a specified wind velocity, the frequency at the terminals of the SCIG is adjusted in such a way that the machine rotates at a speed corresponding to the MPP. The objective of this case is to show the overall performance of the proposed controller under varied conditions of operation. With this purpose, the simulation was carried out considering the wind speed profile and rated wind speed presented in Fig. 5.

In this figure, it's also represented the pitch angle, the tip speed ratio, the coefficient of power conversion, the aerodynamic power, the generator speed and the optimum speed. It is shown that the pitch angle value is set at 0°, the tip speed ratio is equal to 8.1, and the power coefficient Cp is around of 0.47 when the wind speed is lower than 11 m/s. Once the rated speed is greater than 11m/s, the rated power 1 p.u (3 MW) is obtained.

5.2   Tracking Performance of DC Link Voltage and Powers

The Fig. 6 depicts the response of the DC bus voltage. It is noticeable that is regulated at 1380 V. Figure 7 presents the simulation results concerning the grid side: the voltage, the current, the reactive and active powers, respectively. It can be seen that the measured active power tracks very well the reference. Also, the reactive power is equal to its reference which is set to 0. Consequently, the unity power factor is achieved, since the current and the voltage of the grid are in phase.

5.3   Robustness to Parameter Disturbances

In this section, simulation results of the wind turbine SCIG under parameter variation is considered, in order to confirm the robustness of the proposed control. While the variations of the stator and rotor leakage inductances during operation are insignificant, mutual inductance variation should be taking into account due to possible variation of the magnetic permeability of the stator and rotor cores under different operating conditions. Figure 8 shows the simulation results with inductances used in the controller with increase of +50 % from their original values. Besides,
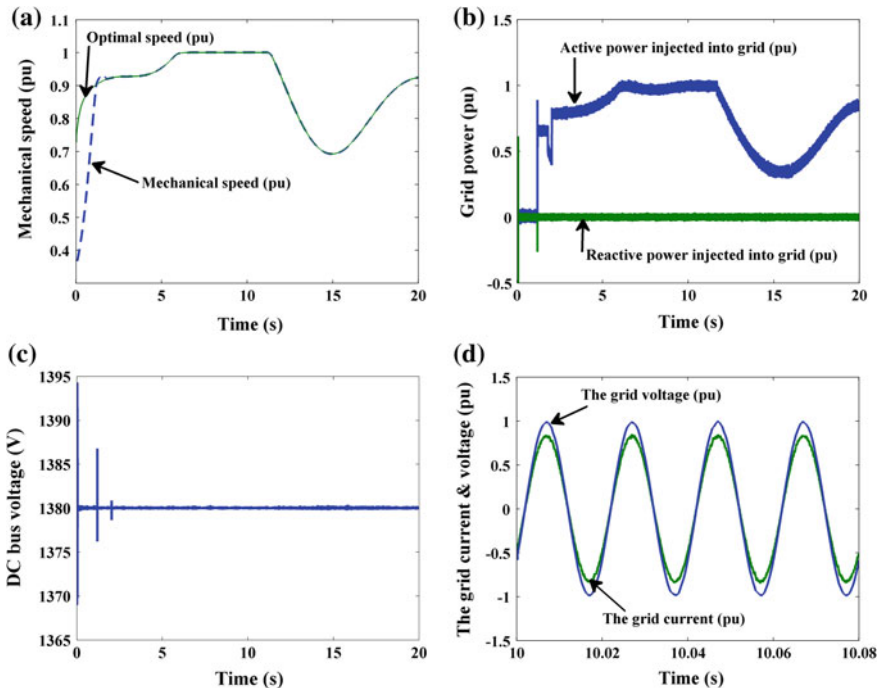

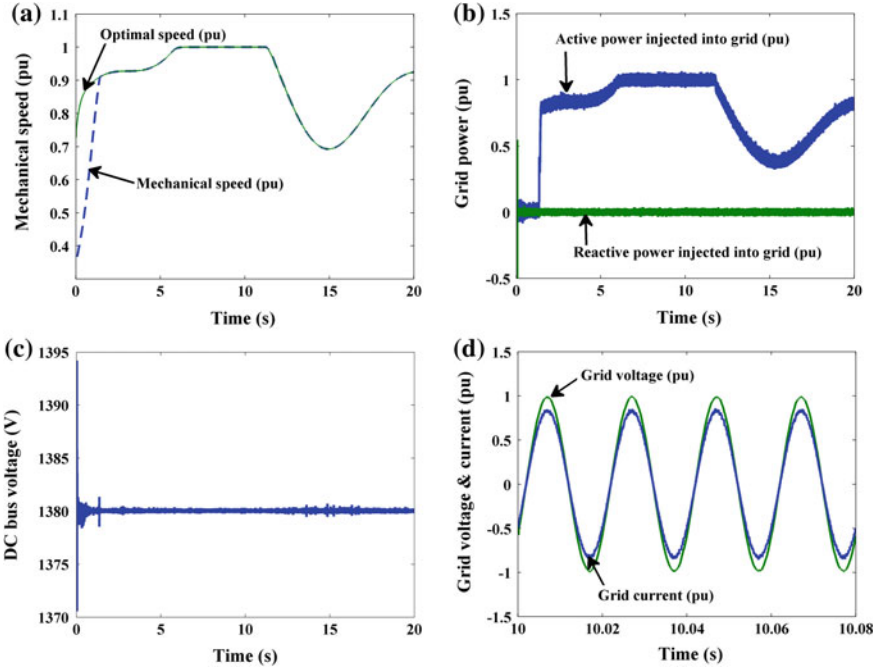**Fig. 8**   Performance of the system under +50 % change in inductance values

Fig. 9 Performance of the system under +50 % change in resistances of stator and rotor

variations of stator and rotor resistances should also be considered. Simulation results with change of resistances of stator and rotor (with the range of +50 %) are shown in Fig. 9. As a result, it can be seen that the proposed scheme can still provide consistent performance even if system parameters have changed.

6 Conclusion

Compared to other types of renewable energy, wind energy system has become a fast increasing energy source in the world; mainly as a consequence of its environmentally friendly, high reliability and cost effectiveness.

WECS based on SCIG is one of promising topology to reduce maintenance costs and to increase mechanical robustness and versatility. Further, it guarantees superior wind power extraction, better efficiency in variable-speed of the wind and improved quality of the energy feed to the grid.

In this context, two simultaneous control objectives have been investigated:

- the maximization of the energy conversion efficiency based SCIG wind turbine
- the regulation of the active and reactive power injected into the grid, to ensure UPF,

To this end, a sliding-mode control strategy, which presents attractive features such as robustness to parametric uncertainties of the different components of the system, has been adopted. The globally and exponentially stability of the derived control laws has been proven by applying Lyapunov stability analysis.

Simulation results have been performed to illustrate successful mathematical analysis and prove the effectiveness of the proposed nonlinear control laws. It can be observed from the simulation study that proposed controllers guarantee good performance in terms of (i) tracking of maximum power, (ii) reactive power regulation to guarantee unity power factor and (iii) robust feedback control solution despite parameter uncertainties and disturbances.

References

1. Alepuz S, Calle A, Busquets-Monge S, Kouro S (2013) Use of stored energy in PMSG rotor inertia for low-voltage ride-through in back-to-back npc converter-based wind power systems. IEEE Trans Indus Electron 60(5):1787–1796
2. Benchagra M, Errami Y, M. Hilal, Maaroufi M, Cherkaoui M, Ouassaid M (2012) New control strategy for inductin generator-wind turbine connected grid. In: International conference on multimedia computing and systems (IEEE-ICMCS), pp 1043–1048
3. Benchagra M, Maaroufi M, Ouassaid M (2014) A performance comparison of linear and nonlinear control of a SCIG-wind farm connecting to a distribution network. Turkish J Electr Eng Comput Sci 22(1):1–11
4. Caliao ND (2011) Dynamic modeling and control of fully rated converter wind turbines. Renew Energy 36:2287–2297
5. Cardenas R, Pena R (2004) Sensorless vector control of induction machines for variable-speed wind energy applications. IEEE Trans Energy Convers 19(1):196–205
6. Chou S, Chia-Tse L, Hsin-Cheng K, Po-Tai C (2014) A low-voltage ride-through method with transformer flux compensation capability of renewable power grid-side converters. IEEE Trans Power Electron 29(4):1710–1719
7. Chen Z, Guerrero JM, Blaabjerg F (2009) A review of the state of the art of power electronics for wind turbines. IEEE Trans Power Electron 24(8):1859–1875
8. Chen J, Jie C, Chunying G (2013) New overall power control strategy for variable-speed fixed-pitch wind turbines within the whole wind velocity range. IEEE Trans Ind Electron 60(7):2652–2660
9. Errami Y, Ouassaid M, Maaroufi M (2013) Modeling and variable structure power control of PMSG based variable speed wind energy conversion system. J Optoelectron Adv Mater 15(12):1248–1255
10. Evangelista C, Fernando V, Paul P (2013) Active and reactive power control for wind turbine based on a MIMO 2-sliding mode algorithm with variable gains. IEEE Trans Energy Convers 28(3):682–689
11. Huang N, He J, Nabeel A, Demerdash O (2013) Sliding Mode observer based position self-sensing control of a direct-drivePMSGwind turbine system fed by NPC converters. In: IEEE international electric machines drives conference (IEMDC), pp 919–925
12. Hu J, Nian H, He BHY, Zhu ZQ (2010) Direct active and reactive power regulation of dfig using sliding-mode control approach. IEEE Trans Energy Convers 25(4):1028–1039
13. Idris NRN, Yatim AHM (2004) Direct torque control of induction machines with constant switching frequency and reduced torque Ripple. IEEE Trans Ind Electron 51(4):758–767
14. Isidori A (1995) Nonlinear control systems, 3rd edn. Springer, New York

15. Jain S, Khorrami F, Fardanesh B (1994) Adaptive nonlinear excitation control of power system withunknown interconnections. IEEE Trans Control Syst Technol 2(4):436–446
16. Kang J, Sul S (1999) New direct torque control of induction motor for minimum torque ripple and constant switching frequency. IEEE Trans Ind Appl 35(5):1076–1082
17. Krstić M, Kanellakopoulos I, Kokotović P (1995) Nonlinear and adaptive control design. Wiley Interscience Publication, New York
18. Lai YS, Chen JH (2001) A new approach to direct torque control of inductionmotor drives for constant inverter switching frequency and torque ripple reduction. IEEE Trans Energy Convers 16(3):220–227
19. Ledesma P, Usaola J (2005) Doubly fed induction generator model for transient stability analysis. IEEE Trans Energy Convers 20(2):388–397
20. Li H, Zhao B, Yang C, Chen HW, Chen Z (2012) Analysis and estimation of transient stability for a grid-connected wind turbine with induction generator. Renew Energy 36:1469–1476
21. Li S, Haskew TA, Swatloski RP, Gathings W (2012) Optimal And Direct-current Vector Control Of Direct-driven Pmsg Wind Turbines. IEEE Trans Power Electron 27(5):2325–2337
22. Li R, Dianguo X (2013) Parallel operation of full power converters in permanent-magnet direct-drive wind power generation system. IEEE Trans Ind Electron 60(4):1619–1629
23. Martinez MI, Susperregui A, Tapia G (2013) Sliding-mode control of a wind turbine-driven doublefed induction generator under non-ideal grid voltages. IET Renew Power Gener 7(4):370–379
24. Melo DFR, Chang-Chien L-R (2014) Synergistic control between hydrogen storage system and offshore wind farm for grid operation. IEEE Trans Sustain Energy 5(1):18–27
25. Meng W, Yang Q, Ying Y, Sun Y, Yang Z, Sun Y (2013) Adaptive power capture control of variablespeed wind energy conversion systems with guaranteed transient and steady-state performance. IEEE Trans Energy Convers 28(3):716–725
26. Mullane A, Lightbody G, Yacamini R (2005) Wind-turbine fault ridethrough enhancement. IEEE Trans Power Syst 20(4):1929–1937
27. Nian H, Song Y (2014) Direct power control of doubly fed induction generator under distorted grid voltage. IEEE Trans Power Electron 29(2):894–905
28. Oliveira DS, Reis MM, Silva CEA, Colado Barreto HS, Antunes FLM, Soares BL (2010) A three-phase high-frequency semicontrolled rectifier for PM WECS. IEEE Trans Power Electron 25(3):677–685
29. Ouassaid M, Nejmi A, Cherkaoui M, Maaroufi M (2008) A Nonlinear backstepping controller for power systems terminal voltage and rotor speed controls. Int Rev Autom Control 3(1):355–363
30. Ouassaid M, Maaroufi M, Cherkaoui M (2010) Decentralized nonlinear adaptive control and stability analysis of multimachine power system. Int Rev Electr Eng 5(6):2754–2763
31. Ouassaid M, Maaroufi M, Cherkaoui M (2012) Observer based nonlinear control of power system using sliding mode control control strategy. Electr Power Syst Res 84(1):135–143
32. Peresada S, Tilli A, Tonielli A (2004) Power control of a doubly fed induction machine via output feedback. Control Eng Prac 12(1):41–57
33. Patil NS, Bhosle YN (2013) A review on wind turbine generator topologies. In: IEEE international conference on power, energy and control (ICPEC), pp 625–629
34. Rajaei AH, Mohamadian M, Varjani AY (2013) Vienna-rectifier-based direct torque control of PMSG for wind energy application. IEEE Trans Ind Electron 60(7):2919–2929
35. Slotine JJE, Li W (1991) Applied nonlinear control. Prentice-Hall, Englewoods Cliffs
36. Souza CL et al (2001) Power system transient stability analysis including synchronous and induction generator. Proc IEEE Porto Power Tech 2:6
37. Susperregui A, Martinez MI, Tapia G, Vechiu I (2013) Second-order sliding-mode controller design and tuning for grid synchronisation and power control of a wind turbine-driven doubly fed induction generator. IET Renew Power Gener 7(5):540–551
38. Tan Y, Wang Y (1998) Augmentation of transient stability using a supperconduction coil and adaptive nonlinear control. IEEE Trans Power Syst 13(2):361–366

39. Tseng K, Huang C-C (2014) High step-up high-efficiency interleaved converter with voltage multiplier module for renewable energy system. IEEE Trans Ind Electron 61(3):1311–1319
40. Utkin VI (1977) Variable structure systems with sliding modes. IEEE Trans Autom Control AC–22:212–222
41. Wu F, Zhang X, Ju P, Sterling MJH (2008) Decentralized nonlinear control of wind turbine with doubly fed induction generator. IEEE Trans Power Syst 23(2):613–621
42. Xu L, Cartwright P (2006) Direct active and reactive power control of DFIG for wind energy generation. IEEE Trans Energy Convers 21(3):750–758